

FUNCTIONAL INTERACTION BETWEEN TRPV4 AND NCS1 AND THE EFFECTS OF PACLITAXEL*

Julio C. Sánchez and Barbara E. Ehrlich

JCS Laboratory of Cell Physiology, Faculty of Health Sciences, Universidad Tecnológica de Pereira, Pereira, Colombia, 660003

BEE Departments of Pharmacology and Cellular and Molecular Physiology, Yale University, New Haven, CT, 06520, U. S. A.

Running title: TRPV4-NCS1 interaction is regulated by PTX

*Corresponding author: Barbara E. Ehrlich, Departments of Pharmacology and Cellular and Molecular Physiology, Yale University, New Haven, CT, 06520, U. S. A.

Number of text pages: 40.

Number of tables: 0.

Number of figures: 9.

Number of references: 74.

Number of words in the *Abstract*: 154.

Number of words in the *Introduction*: 485.

Number of words in the *Discussion*: 1093.

Abbreviations

CIPN: chemotherapy-induced peripheral neuropathy.

NCS1: neuronal calcium sensor 1.

PTX: paclitaxel.

TRPV4: transient receptor potential V4 channel.

InsP₃: inositol trisphosphate.

Ca²⁺: calcium.

KD: knockdown.

OE: overexpressed.

CTR: control.

GSK101: GSK1016790A.

Tg: thapsigargin.

ABSTRACT

Neuronal calcium sensor 1 (NCS1), a calcium-binding protein, and transient receptor potential V4 (TRPV4), a plasma membrane calcium channel, are fundamental in the regulation of calcium homeostasis. The interactions of these proteins and their regulation by paclitaxel (PTX) were investigated using biochemical, pharmacological, and electrophysiological approaches in both a breast cancer epithelial cell model and a neuronal model. TRPV4 and NCS1 reciprocally immunoprecipitated each other, suggesting that they comprise a signaling complex. The functional consequence of this physical association was that TRPV4 currents increased with increased NCS1 expression. Calcium fluxes through TRPV4 correlated with the magnitude of TRPV4 currents and these calcium fluxes depended on NCS1 expression levels. Exposure to PTX amplified the acute effects of TRPV4 expression, currents, and calcium fluxes, but decreased the expression of NCS1. These findings augment the understanding of the properties of TRPV4, the role of NCS1 in the regulation of TRPV4, and the cellular mechanisms of PTX-induced neuropathy.

KEYWORDS: neuronal calcium sensor 1, transient receptor potential V4 channel, paclitaxel, electrophysiology, calcium transients, neuropathic pain, chemotherapy-induced peripheral neuropathy.

SIGNIFICANCE STATEMENT

TRPV4 and NCS1 physically and functionally interact. Increased expression of NCS1 enhances TRPV4 dependent currents, which are further amplified by treatment with the chemotherapeutic drug, paclitaxel, an effect associated with adverse effects of chemotherapy, including neuropathy.

INTRODUCTION

Neuronal Calcium (Ca^{2+}) Sensor (NCS) proteins play essential roles in Ca^{2+} signaling by detecting intracellular Ca^{2+} transients and transducing these signals to other effectors (Ames and Lim, 2012). One of the members of this protein family is NCS1, which binds Ca^{2+} in a high-affinity and low-capacity fashion (Burgoyne et al., 2004). NCS1 is highly expressed in neurons, but is found in most other cell types. NCS1 binds to several proteins including the dopamine receptor 2, the inositol trisphosphate (InsP_3) receptor, and the phosphatidylinositol 4-kinase (Bahi et al., 2003; Haynes et al., 2004; Haynes et al., 2005; Lian et al., 2011; Lian et al., 2014; Schlecker et al., 2006), resulting in functional effects. For example, NCS1 potentiates synaptic transmission through the activation of N-type Ca^{2+} channels (Wang et al., 2001; Weiss and Burgoyne, 2002), and NCS1 affects the dynamics of intracellular Ca^{2+} transients through its enhancement of InsP_3 receptor channel activity (Schlecker et al., 2006).

NCS1 appears to be a critical component of neuropathic pain induced by paclitaxel (PTX), a microtubule-stabilizing compound that is used for cancer chemotherapy (Benbow et al., 2011; Mo et al., 2012). This side effect, which occurs independently of the therapeutic action of PTX on microtubules (Boyette-Davis et al., 2015), is devastating because it is irreversible in nearly half of all patients (Winters-Stone et al., 2016). In cells, treatment with PTX leads to altered Ca^{2+} signaling (Boehmerle et al., 2006) which subsequently induces the activation of a Ca^{2+} -dependent protease, μ -calpain (Benbow et al., 2011; Blachford et al., 2009; Boehmerle et al., 2007). This protease then cleaves several intracellular proteins, including NCS1, affecting cellular responses to activation of the Ca^{2+} signaling pathway (Benbow et al., 2012; Boehmerle

et al., 2006). These changes in Ca^{2+} signaling have been proposed as the initiating event mediating neuronal damage (Boehmerle et al., 2007; Mo et al., 2012). In support of this mechanism, inhibition of calpain, a Ca^{2+} -activated protease, protects against PTX-induced sensory neuropathy *in vivo* (Wang et al., 2004).

TRPV channels are members of a family of channels known as transient receptor potential (TRP) proteins, which play essential roles in numerous processes (Montell et al., 2002), including sensory transduction and nociception (Everaerts et al., 2010a). This study focuses on TRPV4, a member of the vanilloid receptors (Nilius et al., 2003). This channel is expressed in a large variety of cell types (Becker et al., 2005; Benfenati et al., 2007; Liedtke et al., 2000; Phan et al., 2009), and is activated by a variety of stimuli (Nilius et al., 2003; Watanabe et al., 2003b). TRPV4 is also a transducer of inflammatory (Levine and Alessandri-Haber, 2007) and hypotonicity-induced nociceptive responses (Alessandri-Haber et al., 2008), which led to the suggestion that TRPV4 is also related to PTX-induced neuropathic pain (Alessandri-Haber et al., 2004) and contributes to enhanced nociception to hypo-osmotic stimuli in PTX-treated rats (Alessandri-Haber et al., 2005; Alessandri-Haber et al., 2003). Furthermore, the inhibition of TRPV4 can prevent PTX-induced neuropathy in animal models (Boehmerle et al., 2018) and its sensitization induces mechanical hyperalgesia (Costa et al., 2018). Nevertheless, the molecular mechanism leading from PTX administration to TRPV4 activity to pain is unclear. Because both TRPV4 and NCS1 are linked to PTX and neuropathy, we hypothesized that TRPV4 and NCS1 interact and that addition of PTX would alter the inter-relationship.

In this series of experiments, we found that TRPV4 and NCS1 are biochemically linked, that TRPV4 function can be modulated by NCS1, and that the addition of PTX alters this interaction. These results suggest that the TRPV4/NCS1 complex is a component of the pathway, which may be implicated in cell damage associated with the adverse effects of chemotherapy, including neuropathy.

MATERIALS AND METHODS

Cell culture

The human breast carcinoma cell line MDA-MB231 (American Type Culture Collection, Manassas, VA) (**NCI-DTP Cat# MDA-MB-231, RRID:CVCL_0062**), stably transfected to modulate the expression of NCS1 protein (knockdown (KD), overexpressed (OE) and control (CTR) cells), were employed in this study as they are a known cell model that allows the assessment of the effect of different levels of NCS1 expression on different cellular responses with a solid background in our laboratory. These cells were cultured in L-15 Medium (L-15) supplemented with 10% fetal bovine serum, 1% penicillin/streptomycin, and 0.5 mg/l puromycin, in a 5% CO₂ humidified atmosphere in an incubator at 37°C. Cells were transduced with lentivirus to create the desired phenotype and maintained until the start of the experiments. Cells were passaged for use no more than three months after being thawed.

Some experiments were performed also in the human neuroblastoma cell line SH-SY5Y (American Type Culture Collection, Manassas, VA; ATTC CRL2266™), a neuronal cell model, which were cultured in 1:1 DMEM: Ham's F12 medium supplemented with 10% (v/v) heat-inactivated fetal bovine serum, 5% non-essential amino acids, 100 IU penicillin and 50 g/ml streptomycin, in a 5% CO₂ humidified atmosphere in an incubator at 37°C. Cells were passaged for use no more than three months after being thawed.

Cell viability assay

Cell viability was determined by 4,5-dimethylthiazol-2-yl-2,5-diphenyltetrazolium bromide (MTT) assay (Sigma-Aldrich). Briefly, cells were seeded at a density of 2×10^4 cells/well in 96-well plates and incubated in a 37 °C, 5% CO₂ incubator. After overnight

incubation and following PTX exposure, MTT solution (0.5 mg/ml) was added to each well and incubated with the cells for 4 hours. After incubation, the MTT solution was removed and 100 μ l DMSO was added to successfully dissolve the formazan crystals. Absorbance at 570 nm was measured with a microplate reader (ELX800; BioTek Instruments, Inc., Winooski, VT, USA).

RT-PCR and qRT-PCR

Total RNA was extracted from cultured cells using a RNeasy kit (QIAGEN Science, Hilden, Germany) and treated with 55U RNase-free DNase (QIAGEN Science, Hilden, Germany) following the manufacturer's instructions. The purity of the RNA was determined by the 260 nm/280 nm absorbance ratio on a Nanodrop 2000 spectrophotometer (Thermo Fisher Scientific Inc., Waltham, MA).

For RT-PCR, the amplifications were performed using a GeneAmp1Gold RNA PCRCore kit (Applied Biosystems, Foster City, CA) on a Verity1Thermocycler (Applied Biosystems, Foster City, CA) using the following primers: for TRPV4, forward 5'-TGGCTTCTCGCATACCGT-3' and reverse 5'-GGCTCTGGCGTTGGCTTA-3'; and for β -actin, forward 5'-CTGGAACGGTGAAGGTGACA-3' and reverse 5'-AAGGGACTTCCTGTAACAATGCA-3'. The amplified RNA was checked by agarose gel electrophoresis and visualized on a GEL DOC XRp1 (BIORAD Hercules, CA). The amplified transcripts were sequenced to confirm homology with the predicted fragment.

RT-qPCR was developed by StepOnePlus™ Real-Time PCR System (Applied Biosystems), transforming RNA in DNAc using TaqMan® RNA-to-CT TM 1-Step Kit (Applied Biosystems) following the manufacturer instructions. The genes that were evaluated were TRPV4 (Hs01099348_m1) and β -actin (Hs01060665_g1), as a control.

Results were analyzed using the $2^{-\Delta\Delta C_t}$ method and presented as relative gene expression normalized to the average cycle threshold for the β -actin gene.

Western blotting

Cultured MDA-MB231 cells were lysed with protein lysis buffer MPER (Thermo Fisher Scientific Inc., Waltham, MA), with the addition of a protease inhibitor cocktail (P2714, Sigma Aldrich, 1:100), and centrifuged at 10,000 g for 15 min at 4°C. Cell lysates containing 20 mg of protein were separated by SDS-PAGE, followed by electrophoretic transfer onto PVDF membranes. The membranes were cut in three sections, where each section included the molecular weight of the target protein, and each section was incubated with the corresponding primary antibody. The primary antibodies used were: anti-TRPV4 (Alomone, Jerusalem, Israel, 1:500) (**Alomone Labs Cat# ACC-034, RRID:AB_2040264**), anti-NCS1 (FL190, Santa Cruz Biotechnology, Santa Cruz, CA, 1:10000) (**Santa Cruz Biotechnology Cat# sc-13037, RRID:AB_649907**), and anti- β -actin (Santa Cruz Biotechnology, Santa Cruz, CA, 1:2000) (**Santa Cruz Biotechnology Cat# sc-130301, RRID:AB_2223360**). Membranes were incubated with primary antibodies overnight at 4°C. After incubation with rabbit secondary antibody (1:20000) (**Bio-Rad Cat# 166-2408EDU, RRID:AB_11125345**) for TRPV4 and NCS1, and mouse secondary antibody (1:20000) (**Bio-Rad Cat# 170-6516, RRID:AB_11125547**) for β -actin, for 2 h at room temperature, the bands were visualized by an enhanced chemiluminescence system.

Co-Immunoprecipitation (Co-IP)

MDA-MB231 cells were lysed with protein lysis buffer MPER (Thermo Fisher Scientific Inc., Waltham, MA), with the addition of a protease inhibitor cocktail (P2714, Sigma

Aldrich, 1:100), and centrifuged at 10,000 g for 15 min at 4°C. The supernatant was incubated with anti-NCS1 antibody (FL190, Santa Cruz Biotechnology, Santa Cruz, CA, 1: 5000) for 1 h at 4°C and then precipitated employing protein-A magnetic beads (PureProteome, EMD Millipore, Billerica, MA) by incubating for 1 h at 4°C, following the manufacturer's instructions. Beads were washed and then eluted, and protein levels were quantified using Western blot analysis, employing anti-NCS1 (FL190, Santa Cruz Biotechnology, Santa Cruz, CA, 1: 10000) or anti-TRPV4 (Alomone, Jerusalem, Israel, 1:500). The co-IP experiments were also conducted in the reverse mode, employing anti-TRPV4 (Alomone, Jerusalem, Israel, 1:500) to induce immunoprecipitation and then using anti-NCS1 and anti-TRPV4 in Western blot analysis to assess the interactions between NCS1 and TRPV4.

Electrophysiology

Whole-cell or inside-out patch-clamp technique was used to record membrane currents (voltage clamp) in MDA-MB231 cells. Cells were placed in a recording chamber that was attached to an inverted microscope (TE2000U, Nikon, Tokyo, Japan). Patch pipettes (Sutter Instruments, Novato, CA) were pulled to resistances of 5–8 MΩ (P-97, Sutter Instruments, Novato, CA) and then polished. After a seal of resistance greater than 5 GΩ was obtained, recordings of membrane currents were made using the whole-cell mode or the inside out mode. An Axopatch 200B amplifier with a CV203BU headstage (Molecular Devices, Union City, CA) was used. Voltage clamp signals were generated by a Digidata 1440A interface (Molecular Devices, Union City, CA). Acquisition and analysis of signals were made using pCLAMP 10.0 (Molecular Devices, Union City, CA). All experiments were performed at 20 °C. The standard external

solution, which was superfused at 25°C, contained (mM): 140 NaCl, 5 KCl, 2 CaCl₂, 1 MgCl₂, 15 HEPES, and 10 glucose, with pH adjusted to 7.4 with NaOH. The standard pipette solution contained (mM): 110 KCl, 20 K-gluconate, 20 NaCl, 0.1 CaCl₂, 4 MgCl₂, 10 HEPES, 5 glucose, with pH adjusted to 7.1 with NaOH at 25°C. In Na⁺-free solutions, Na⁺ was replaced with equimolar concentrations of NMDG. In order to chelate contaminant traces of Ca²⁺, EGTA (1mM) was added to the Ca²⁺-free solutions.

Ca²⁺ measurements

Cultured cells in suspension were loaded with Fura-2 AM (5 mM; Thermo Fisher Scientific Inc., Waltham, MA) by incubation in HBS for 30 min at 20°C followed by 15 min at 37°C. Cell suspensions were then centrifuged, and the cells were resuspended in the appropriate experimental medium before being transferred to a 1 mL cuvette. Fluorometer measurements were made for 300 sec (FP-6500 spectrophotometer, Jasco, Tokyo, Japan); the temperature was maintained at 37°C, and magnetic stirring was implemented during the measurements. The dye was alternately excited at 380 and 340 nm, and the fluorescence emission was measured at 510 nm. The 380 nm/340nm signal ratio was calibrated before every experiment (Grynkiewicz et al., 1985). Briefly, the fluorescence ratio was measured in HBS lacking Ca²⁺, supplemented with EGTA (1 mM) and in a 2 mM Ca²⁺ containing HBS supplemented with ionomycin (300 nM), a Ca²⁺ concentration at which Fura-2 is saturated. Maximal and minimal ratios (R_{max} and R_{min}) were obtained under these two conditions, and the [Ca²⁺]_i values were derived using the following equation:

$$[Ca^{2+}]_i = K_d (R - R_{min} / R_{max} - R) (Sf_2 / Sb_2),$$

where K_d is the dissociation constant for Fura-2, which was 224 nM in the present study according to measurements obtained under similar experimental conditions (Grynkiewicz et al., 1985), R is the experimentally measured ratio, Sf_2 is the fluorescence measured at 380 nm in the Ca^{2+} -free conditions, and Sb_2 is the fluorescence measured at 380 nm with saturating Ca^{2+} (2 mM).

Isolation and purification of Ca^{2+} -free NCS1 protein

NCS1 was produced by overexpression of rat NCS1 in Stratagene BL21(DE3) Codon Plus RIL competent *E. coli* cells transformed with a pET21-a+ bacterial expression vector subcloned with rat NCS1 cDNA. The published purification protocol (Zozulya et al., 1995) was modified slightly. Briefly, cells were grown at 37° C in 2 L baffled flasks with 1 L LB Broth (Miller) plus ampicillin (100 ug/mL), and chloramphenicol (30 ug/mL). At an OD_{595 nm} 0.5-0.7, overexpression was induced with 1 mM isopropyl-D-thiogalactoside (IPTG) and allowed to incubate for 3 hours. Cells were harvested by centrifugation at 3000 rpm for 3 min at 4° C and resuspended in 10 mL of 50 mM HEPES, 100 mM KCl, 1 mM *tris* (2-carboxyethyl)phosphine (TCEP), 1 mM MgCl₂, and 10 mM CaCl₂ at pH 7.5.

Bacteria expressing recombinant NCS1 were lysed in a buffer containing lysozyme (Sigma Aldrich, 2 mg/mL), DNase I (from bovine pancreas, Sigma Aldrich, 2 uL/1 mL of 2 mg/mL stock) and subjected to three freeze-thaw cycles using ethanol and dry ice. The lysate was homogenized by sonication for 2 minutes on ice using a 50% duty cycle and an output level of 5. The lysate was then clarified by centrifugation at 40,000 x g (20,000 rpm, 1 hour, 4 C) and sonicated again to reduce sample viscosity. The supernatant was then filtered with a 0.22 um Steriflip filter unit before hydrophobic

interaction chromatography (HIC). HIC was performed using a GE Healthcare HiTrap Phenyl HP 5 mL column equilibrated with 50 mM HEPES, 100 mM KCl, 1 mM TCEP, 1 mM MgCl_2 , and 10 mM CaCl_2 at pH 7.5. After the application of the lysate three times through the column, the column was washed with ten volumes of the same buffer used to equilibrate the column. Recombinant protein was eluted using 50 mM HEPES, 100 mM KCl, 1 mM TCEP, 1 mM MgCl_2 , and 50 mM EDTA at pH 7.5. The protein was collected in 25 x 1 mL fractions, evaluated for purity by SDS-PAGE and Coomassie stain.

Recombinant protein fractions were pooled to be desalted using a Bio-Rad Econo-Pac 10DG column with 50 mM HEPES and 100 mM KCl at pH 7.5 as the exchange buffer. NCS1 was then dialyzed through a series of buffers in a Pierce Slide-A-Lyzer 7K MWCO cassette: 1 L 10 mM EDTA at pH 2 for 1.5 hours; 1 L MilliQ water for 1.5 hours; 1 L 10 mM HEPES at pH 7.4 for 1.5 hours; and lastly, 1 L 50 mM HEPES, 100 mM KCl, 0.5 mM TCEP at pH 7.2 overnight. Dialysis was performed using only plastic containers to prevent Ca^{2+} contamination from glass. The protein was concentrated to the desired concentration using a Millipore Ultracel 3 K Amicon Ultra-15 centrifugal filter device.

Statistical analysis

Results are presented as the mean \pm standard deviation (SD), and n represents the number of cells tested in the electrophysiological experiments or the number of different cell batches employed in all other essays. Analysis was performed employing GraphPad 8.4.3 software. Statistically significant differences were determined using one-way ANOVA test or two-way ANOVA test according to the number of variables,

employing Bonferroni post hoc test, where applicable. A $p < 0.05$ was considered significant, but the exact value of p was reported in each analysis.

RESULTS

Effects of PTX in cell survival

PTX, at the concentrations and times of exposure that were employed in this study, did not have effects on survival of either MDA-MB231 or SH-SY5Y. The percentage of survival was maintained near 100% in all the tests performed following 1-min and 6-hours PTX exposure ($n=10$ in each case), and there were no significant differences.

Expression of TRPV4, regulation by NCS1 and effects of PTX on protein levels

In order to evaluate the level of expression of TRPV4, RT-PCR and Western Blot (WB) experiments were conducted in MDA-MB231 cells with different levels of expression of NCS1. The expression of TRPV4 was higher in cells that over-expressed NCS1 (OE) and lower in cells that under-expressed this protein (KD) in comparison with controls (CTR) when measured as either mRNA (Fig 1A and 1B) or protein expression (Fig 1C). Similar results were obtained using eight different batches of cells (Fig 1D). In RT-PCR experiments, the transcript observed matched the expected 431 bp size for TRPV4 and 140 bp size for β -actin, which was amplified as a control, as found on the Primer-BLAST website (<http://www.ncbi.nlm.nih.gov/tools/primer-blast>) provided by the National Center for Biotechnology Information (NCBI). The identity of the PCR products was confirmed by sequence analysis. In WB experiments, the expression of TRPV4 was confirmed by the identification of a band at 100 kDa, as expected for TRPV4 in other cell types. The expression of β -actin was used as a control.

A 6-hour pretreatment with PTX (1 μ M) significantly increased the TRPV4 protein levels and decreased NCS1 protein levels (Fig 1E and F). The concentrations of PTX were

chosen by the respective concentration-response curves on TRPV4 current magnitude (Sanchez et al., 2020) and are comparable to concentrations used in our prior experiments on the InsP₃ receptor (Benbow et al., 2012; Mo et al., 2012). We recently reported similar results in SH-SY5Y cells (Sanchez et al., 2020).

Physical association of TRPV4 and NCS1

Co-IPs were conducted to examine the molecular association between TRPV4 and NCS1 proteins in MDA-MB231 CTR (normal NCS1 expression levels). TRPV4 was detected by WB in immunoprecipitates pulled down by anti-NCS1 and NCS1 was detected by WB in immunoprecipitates pulled down by anti-TRPV4 (Fig 2A; n=5). These molecular interactions between TRPV4 and NCS1 were not affected by the presence of PTX (1 μ M) (Fig 2B; n=3).

Electrophysiological experiments and effects of NCS-1 and PTX on I_{TRPV4}

A descending ramp protocol was used to determine whole-cell currents in the MDA-MB231 CTR cells. Specifically, the membrane potential was stepped from the resting potential of -60 mV to $+100$ mV and decreased to -100 mV over 2 seconds. Following background current subtraction, GSK1016790A (GSK101, 100 nM), a specific and potent TRPV4 activator (Thorneloe et al., 2008), elicited a current, which exhibited voltage dependence with a reversal potential (E_{rev}) of $+27 \pm 5$ mV ($n = 12$) (Fig 3A and B). Outward and inward rectification was noted from the traces. Both outward and inward components of these currents were decreased by HC-067047 (50 nM), a specific inhibitor of TRPV4 channels (Everaerts et al., 2010b), which confirmed its identity as I_{TRPV4} (Fig 4D). These results are in agreement with results reported previously in SH-SY5Y cells (Sanchez et al., 2020).

To evaluate whether the levels of expression of NCS1 affected I_{TRPV4} , experiments were done using KD and OE cell lines. The currents were higher in OE cells and lower in KD cells in comparison to CTR cells (Fig 3A and B), as shown in a single representative cell (Fig 3A) or the average of 15 cells (Fig 3B and C). As with the CTR cell lines, the addition of HC-067047 (50 nM) inhibited the currents with all levels of NCS1 expression (Fig 3D, n=6).

To assess the effects of PTX (1 μ M) on I_{TRPV4} , this agent was added to the extracellular solution 1 minute before applying the ramp protocol and GSK101 and recording the corresponding current-voltage relationship in MDA-MB231 CTR cells (Fig 4A). The acute effect of PTX was also evaluated at fixed voltages (-60 mV and + 60 mV) after GSK101 treatment (Fig 4B). PTX increased the magnitude of both the outward and inward current density (Fig 4A, B and C). In the absence of GSK101, the addition of PTX did not alter the basal current; addition of GSK101 was necessary to evoke the current (Fig 4B). Note that the effects were fully reversible when the agent was washed out from the extracellular solution (Fig 4B, after the largest arrow indicating washout). The chronic effects of this agent were also evaluated (Fig 4D); current density increased after a 6-hour exposure to PTX in comparison to CTR, and this effect was more pronounced than after the acute treatment. Previously, we found similar results in SH-SY5Y cells (Sanchez et al., 2020).

These experiments were also conducted in MDA-MB231 KD and OE cells (Fig 4C and D). Following either 1-minute (Fig 4C) or 6-hour exposure (Fig 4D), PTX increased the current density in OE cells, but failed to do so in KD cells. The effect of chronic

exposure to PTX in OE cells was amplified, as in CTR cells. Both acute and chronic effects of PTX were higher in OE cells compared to CTR cells.

In order to assess the direct effect of NCS1 on I_{TRPV4} , inside-out excised patches were generated from MDA-MB231 CTR cells. This configuration is necessary because the protein cannot cross the plasma membrane. To determine the protein concentration to be used, a concentration-response curve was constructed, assessing the effect at -60 mV and +60 mV, and the minimal concentration that evoked the maximal response was employed. NCS1 (10 μ M) was added to the extracellular solution 1 minute before recording the currents. GSK101 (100 nM) was added to activate TRPV4 channels (Fig 5B and C) and open probability (P_o , a measure of the proportion of the total recording time that an ion channel spends in its open state) and current-voltage curves were derived (Fig 5D). TRPV4 P_o was significantly increased by NCS1 (Fig 5D). Inward and outward conductances were 51.9 and 97.1 pS respectively (Fig 5E), which are consistent with the expected values for TRPV4 currents (Nilius et al., 2004; Zheng et al., 2013) and both inward and outward currents were significantly increased by NCS1 (Fig 6E and F). Control experiments showed that the behavior of TRPV4 in MDA-MB231 OE and KD cells in basal conditions and in response to PTX were indistinguishable (data not shown).

These series of experiments were also performed in SH-SY5Y cells and the results were similar to those described in MDA-MB231 CTR cells (Fig 6). The effect of PTX was also observed at the single-channel level using inside-out patch experiments. After a 1-minute exposure, in the presence and the absence of NCS1 (10 μ M), PTX increased TRPV4 P_o (Fig 7 A and C) and conductance (Fig 7D), although the P_o was

already near maximum. Addition of NCS1 still induced an increase, but again, the baseline P_o was near maximum (Fig 7B and C). A similar effect was observed on channel conductance after the addition of PTX (Fig 7D). All these effects of NCS-1 were non reversible, since after washing-out the protein they remained.

These single-channel recordings were also performed in SH-SY5Y cells (Fig 8). These cells exhibited the expected conductance and NCS1 and PTX had the same effects described in MDA-MB231 CTR cells and were also non reversible.

Ca²⁺ measurements and effects of PTX on TRPV4-dependent Ca²⁺ increase

The effects of GSK101 on intracellular Ca²⁺ concentrations were recorded using suspensions of MDA-MB231 KD, CTR and OE cells. This agent significantly increased the intracellular Ca²⁺ concentrations in all three cell lines, but the increase was higher in OE cells and lower in KD cells in comparison to CTR cells (Fig 9A and B). This increase was inhibited by HC-067047 in all three cell lines, confirming that TRPV4 was the responsible pathway for Ca²⁺. To determine the source of this increase in intracellular Ca²⁺ levels, cells were either treated with thapsigargin (Tg, 1 μ M, 30 min preincubation in Ca²⁺-free extracellular solution) to deplete intracellular stores or resuspended in Ca²⁺-free extracellular solution before treatment with GSK101. Whereas Tg did not affect the GSK101-induced [Ca²⁺]_i increases, there was a suppression of the response in the Ca²⁺-free extracellular solution in all cells tested (Fig 9B).

The GSK101-induced Ca²⁺ increase was augmented by PTX (Fig 9A and C). The PTX effect was more pronounced when cells were exposed to these agents for 6 hours (Fig 9C). PTX effects were similar in CTR and OE cells, but it failed to affect GSK101-

induced $[Ca^{2+}]_i$ increase in KD cells after either acute or chronic exposure (Fig 9C).
These results are similar to those reported in SH-SY5Y cells (Sanchez et al., 2020).

DISCUSSION

This study provides evidence for the expression and activity of TRPV4 channels in MDA-MB231 cells. In addition, this study presents findings that support the regulation of TRPV4 channel expression and function by NCS1, which can be affected by PTX, in the same cells and also in the neuronal cell line SH-SY5Y. These effects may help to understand better the mechanisms through which PTX induces cell damage and neuropathy (Boyette-Davis et al., 2015; Mielke et al., 2006).

The expression of TRPV4 was shown at both gene and protein levels in these cells. Furthermore, the expression of TRPV4 was dependent on the levels of NCS1 expression, and co-IP experiments showed that there is a physical association between NCS1 and TRPV4 proteins.

NCS1 can form molecular complexes with several proteins and can regulate several signaling pathways. These interactions can explain the regulatory effect of NCS1 on processes ranging from neurotransmission and synaptic plasticity in neurons (Dason et al., 2012; Dason et al., 2009; Ng et al., 2015; Romero-Pozuelo et al., 2014) to some non-neuronal mechanisms and also the role of NCS1 in a variety of pathophysiological processes (Boeckel and Ehrlich, 2018). NCS1 is a regulator of ion channels, particularly Ca^{2+} channels (Kawakami et al., 2012; Lian et al., 2014; Weiss et al., 2010; Yan et al., 2014). However, until now, TRPV4 had not been associated with NCS1 function, although TRPV4 has been implicated in processes in which NCS1 is a regulator, such as neurotransmission (Cao et al., 2009; Fichna et al., 2015; Li et al., 2013).

Here we show that NCS1 can modulate TRPV4 channel electrophysiological features. In this study TRPV4 expression and channel function was comparable to previously reported values (Everaerts et al., 2010a; Nilius et al., 2003; Sanchez et al., 2020; Vriens

et al., 2009; Watanabe et al., 2003a) in other cell types. Importantly, we found that elevated levels of NCS1 were associated with a higher density of I_{TRPV4} , and lower levels of NCS1 were associated with lower density of the currents. Physiologically, TRPV4 is considered to be a polymodal channel because it can be activated by cell swelling, heat, pH acidic, and by chemical ligands such as cannabinoids (Nilius et al., 2003; Watanabe et al., 2003b) and it can be modulated by protein kinase C and other signaling systems (Fan et al., 2009; Mamenko et al., 2013; Peng et al., 2010; Saifeddine et al., 2015). NCS1 is associated with many of these pathways (Burgoyne and Haynes, 2015; Pandalaneni et al., 2015) and thus, may be a critical regulatory component, which is also suggested by the physical association that co-immunoprecipitation experiments confirmed.

The level of NCS1 expression directly correlates with the level of TRPV4 expression, at least in MDA-MB231 cells. Furthermore, NCS1 increases TRPV4 P_o , indicating that NCS-1 affects TRPV4 channel gating, but it also affects the magnitude of conductance, indicating an effect on channel permeability. The molecular mechanisms through which NCS1 affects these functional features of TRPV4 need to be explored in future studies. These results suggest that, physiologically, NCS-1 regulates the activity of TRPV4. When TRPV4 activity is enhanced by NCS1, there is an increased Ca^{2+} influx which, in turn down-regulates the effectiveness of NCS1 function by promoting calpain activity, a Ca^{2+} -dependent protease. Activation of calpain degrades NCS1 and decreases Ca^{2+} influx into the cell in process similar to the mechanism shown for the interactions between NCS1 and the $InsP_3$ receptor, a Ca^{2+} channel in the endoplasmic reticulum membrane, which regulates Ca^{2+} flux into the cytoplasm (Boehmerle et al., 2006;

Boehmerle et al., 2007; Wang et al., 2004). This calpain-dependent process can down-regulate NCS1 activity and thus, modulate the action of all proteins that depend on NCS1 activation.

The relationship between NCS1, as an intracellular Ca^{2+} sensor, and TRPV4 channels, as a crucial Ca^{2+} plasma membrane channel, and the InsP_3 receptor, an intracellular Ca^{2+} release channel, is intriguing because both channels are regulated by intracellular Ca^{2+} (Bezprozvanny et al., 1991; Strotmann et al., 2003; Watanabe et al., 2003a), and both channels are regulated by NCS1 (Sanchez et al., 2020; Schlecker et al., 2006). The combination of all components leads to the potential for reciprocal regulation.

The fact that PTX can affect TRPV4 and NCS1 functioning is potentially important because this drug has been commonly used as an anticancer chemotherapeutic agent to treat solid tumors, such as breast, ovarian, and lung cancers (Baird et al., 2010; Chang and Garrow, 1995; Sarosy et al., 2010). However, PTX has a serious side effect, peripheral neuropathy, that can be incapacitating and may lead to the suspension of treatment (Mielke et al., 2006; Pachman et al., 2011). The dose of PTX employed in this study, chosen by the respective concentration-response curves on TRPV4 current magnitude in SH-SY5Y cells (Sanchez et al., 2020) is similar to concentrations used in previous studies (Benbow et al., 2012; Mo et al., 2012). Although it is difficult to compare with the doses employed in all clinical treatments which use different therapeutic schemes tailored to patient needs, (Andriguetti et al., 2017), the level of PTX used in these experiments is close to values measured in patients (Boehmerle et al., 2006; Rowinsky et al., 1999).

The mechanism by which PTX produces neurotoxicity is different from its therapeutic action, which is mediated by stabilizing microtubule polymers (Schiff et al., 1979). Although the exact mechanisms underlying neurotoxicity are not established, it is known that NCS1 is involved in this response (Boehmerle et al., 2006; Boehmerle et al., 2007; Mo et al., 2012), as PTX increases the activity of the NCS1-InsP₃ receptor complex (Boehmerle et al., 2006; Boehmerle et al., 2007; Nguyen et al., 2019; Wang et al., 2004). The initial increase in cytoplasmic Ca²⁺ may also occur through activation of other Ca²⁺ pathways such as TRP channels (Alessandri-Haber et al., 2004; Materazzi et al., 2012). The findings of this study confirm that PTX increases currents mediated by TRPV4 channels and increases Ca²⁺ influx. This mechanism may contribute to the initial PTX-induced Ca²⁺ increase that produces calpain activation, causes neurotoxicity, and leads to neuropathy. Cytosolic Ca²⁺ oscillations induced by PTX by binding to NCS1 and subsequent positive modulation of the InsP₃ receptor is likely also potentiated in a TRPV4-dependent manner; furthermore, TRPV4 can be modulated directly by InsP₃ (Takahashi et al., 2014), which is another potential pathway to this mechanism. This increase in cytoplasmic Ca²⁺ will lead to the activation of Ca²⁺-activated proteases, and if prolonged, will result in cell malfunction and, ultimately, neuronal damage.

Similar to reports in dorsal root ganglion neurons (Matsumura et al., 2014) and SH-SY5Y cells (Sanchez et al., 2020), PTX augmented the expression of TRPV4 protein, which can contribute to the enhanced activity of TRPV4 induced by PTX. However, PTX is also associated with decreased levels of NCS1, as shown previously (Benbow et al., 2012). We hypothesize that the increase in the TRPV4 expression levels after chronic treatment with PTX is a compensatory effect to maintain cell signaling. The effect of

PTX on gene expression of TRPV4 and NCS1 proteins may be independent and the possible interaction between NCS1 and TRPV4 protein levels could not prevent that influence. In other words, the inhibitory effect of PTX on NCS1 levels does not affect the stimulatory effect of PTX on TRPV4 expression, as suggested by the results presented here.

Presently, there are no approved treatments to prevent or treat the side effects of PTX administration in chemotherapy. Understanding the effects of PTX on Ca^{2+} homeostasis will assist in the design of new therapeutic strategies to target drug-induced neuropathy and, possibly, to optimize the usage of these drugs.

ACKNOWLEDGMENTS

We thank Laura Muñoz for technical assistance and Larry Huynh for NCS1 isolation.

This study was funded in part by NIH grant 5P01DK057751 (B.E.E).

AUTHORSHIP CONTRIBUTIONS

Both authors, JCS and BEE, contribute significantly to the conception and design of the study. JCS performed the experiments. Both authors participated in the analysis and interpretation of data, drafted the article, revised it, and approved it.

REFERENCES

- Alessandri-Haber N, Dina OA, Joseph EK, Reichling DB and Levine JD (2008)
Interaction of transient receptor potential vanilloid 4, integrin, and SRC tyrosine kinase in mechanical hyperalgesia. *J Neurosci* **28**(5): 1046-1057.
- Alessandri-Haber N, Dina OA, Yeh JJ, Parada CA, Reichling DB and Levine JD (2004)
Transient receptor potential vanilloid 4 is essential in chemotherapy-induced neuropathic pain in the rat. *J Neurosci* **24**(18): 4444-4452.
- Alessandri-Haber N, Joseph E, Dina OA, Liedtke W and Levine JD (2005) TRPV4 mediates pain-related behavior induced by mild hypertonic stimuli in the presence of inflammatory mediator. *Pain* **118**(1-2): 70-79.
- Alessandri-Haber N, Yeh JJ, Boyd AE, Parada CA, Chen X, Reichling DB and Levine JD (2003) Hypotonicity induces TRPV4-mediated nociception in rat. *Neuron* **39**(3): 497-511.
- Ames JB and Lim S (2012) Molecular structure and target recognition of neuronal calcium sensor proteins. *Biochim Biophys Acta* **1820**(8): 1205-1213.
- Andrigueti NB, Raymundo S, Antunes MV, Perassolo MS, Verza SG, Suyenaga ES and Linden R (2017) Pharmacogenetic and Pharmacokinetic Dose Individualization of the Taxane Chemotherapeutic Drugs Paclitaxel and Docetaxel. *Curr Med Chem* **24**(33): 3559-3582.
- Bahi N, Friocourt G, Carrie A, Graham ME, Weiss JL, Chafey P, Fauchereau F, Burgoyne RD and Chelly J (2003) IL1 receptor accessory protein like, a protein involved in X-linked mental retardation, interacts with Neuronal Calcium Sensor-1 and regulates exocytosis. *Hum Mol Genet* **12**(12): 1415-1425.

- Baird RD, Tan DS and Kaye SB (2010) Weekly paclitaxel in the treatment of recurrent ovarian cancer. *Nat Rev Clin Oncol* **7**(10): 575-582.
- Becker D, Blase C, Bereiter-Hahn J and Jendrach M (2005) TRPV4 exhibits a functional role in cell-volume regulation. *J Cell Sci* **118**(Pt 11): 2435-2440.
- Benbow JH, DeGray B and Ehrlich BE (2011) Protection of neuronal calcium sensor 1 protein in cells treated with paclitaxel. *J Biol Chem* **286**(40): 34575-34582.
- Benbow JH, Mann T, Keeler C, Fan C, Hodsdon ME, Lolis E, DeGray B and Ehrlich BE (2012) Inhibition of paclitaxel-induced decreases in calcium signaling. *J Biol Chem* **287**(45): 37907-37916.
- Benfenati V, Amiry-Moghaddam M, Caprini M, Mylonakou MN, Rapisarda C, Ottersen OP and Ferroni S (2007) Expression and functional characterization of transient receptor potential vanilloid-related channel 4 (TRPV4) in rat cortical astrocytes. *Neuroscience* **148**(4): 876-892.
- Bezprozvanny I, Watras J and Ehrlich BE (1991) Bell-shaped calcium-response curves of Ins(1,4,5)P₃- and calcium-gated channels from endoplasmic reticulum of cerebellum. *Nature* **351**(6329): 751-754.
- Blachford C, Celic A, Petri ET and Ehrlich BE (2009) Discrete proteolysis of neuronal calcium sensor-1 (NCS-1) by mu-calpain disrupts calcium binding. *Cell Calcium* **46**(4): 257-262.
- Boeckel GR and Ehrlich BE (2018) NCS-1 is a regulator of calcium signaling in health and disease. *Biochim Biophys Acta Mol Cell Res* **1865**(11 Pt B): 1660-1667.

- Boehmerle W, Huehnchen P, Lee SLL, Harms C and Endres M (2018) TRPV4 inhibition prevents paclitaxel-induced neurotoxicity in preclinical models. *Exp Neurol* **306**: 64-75.
- Boehmerle W, Splittgerber U, Lazarus MB, McKenzie KM, Johnston DG, Austin DJ and Ehrlich BE (2006) Paclitaxel induces calcium oscillations via an inositol 1,4,5-trisphosphate receptor and neuronal calcium sensor 1-dependent mechanism. *Proc Natl Acad Sci U S A* **103**(48): 18356-18361.
- Boehmerle W, Zhang K, Sivula M, Heidrich FM, Lee Y, Jordt SE and Ehrlich BE (2007) Chronic exposure to paclitaxel diminishes phosphoinositide signaling by calpain-mediated neuronal calcium sensor-1 degradation. *Proc Natl Acad Sci U S A* **104**(26): 11103-11108.
- Boyette-Davis JA, Walters ET and Dougherty PM (2015) Mechanisms involved in the development of chemotherapy-induced neuropathy. *Pain Manag* **5**(4): 285-296.
- Burgoyne RD and Haynes LP (2015) Sense and specificity in neuronal calcium signalling. *Biochim Biophys Acta* **1853**(9): 1921-1932.
- Burgoyne RD, O'Callaghan DW, Hasdemir B, Haynes LP and Tepikin AV (2004) Neuronal Ca²⁺-sensor proteins: multitalented regulators of neuronal function. *Trends Neurosci* **27**(4): 203-209.
- Cao DS, Yu SQ and Premkumar LS (2009) Modulation of transient receptor potential Vanilloid 4-mediated membrane currents and synaptic transmission by protein kinase C. *Mol Pain* **5**: 5.

- Chang AY and Garrow GC (1995) Pilot study of vinorelbine (Navelbine) and paclitaxel (Taxol) in patients with refractory breast cancer and lung cancer. *Semin Oncol* **22**(2 Suppl 5): 66-70; discussion 70-61.
- Costa R, Bicca MA, Manjavachi MN, Segat GC, Dias FC, Fernandes ES and Calixto JB (2018) Kinin Receptors Sensitize TRPV4 Channel and Induce Mechanical Hyperalgesia: Relevance to Paclitaxel-Induced Peripheral Neuropathy in Mice. *Mol Neurobiol* **55**(3): 2150-2161.
- Dason JS, Romero-Pozuelo J, Atwood HL and Ferrus A (2012) Multiple roles for frequenin/NCS-1 in synaptic function and development. *Mol Neurobiol* **45**(2): 388-402.
- Dason JS, Romero-Pozuelo J, Marin L, Iyengar BG, Klose MK, Ferrus A and Atwood HL (2009) Frequenin/NCS-1 and the Ca²⁺-channel alpha1-subunit co-regulate synaptic transmission and nerve-terminal growth. *J Cell Sci* **122**(Pt 22): 4109-4121.
- Everaerts W, Nilius B and Owsianik G (2010a) The vanilloid transient receptor potential channel TRPV4: from structure to disease. *Prog Biophys Mol Biol* **103**(1): 2-17.
- Everaerts W, Zhen X, Ghosh D, Vriens J, Gevaert T, Gilbert JP, Hayward NJ, McNamara CR, Xue F, Moran MM, Strassmaier T, Uykai E, Owsianik G, Vennekens R, De Ridder D, Nilius B, Fanger CM and Voets T (2010b) Inhibition of the cation channel TRPV4 improves bladder function in mice and rats with cyclophosphamide-induced cystitis. *Proc Natl Acad Sci U S A* **107**(44): 19084-19089.

- Fan HC, Zhang X and McNaughton PA (2009) Activation of the TRPV4 ion channel is enhanced by phosphorylation. *J Biol Chem* **284**(41): 27884-27891.
- Fichna J, Poole DP, Veldhuis N, MacEachern SJ, Saur D, Zakrzewski PK, Cygankiewicz AI, Mokrowiecka A, Malecka-Panas E, Krajewska WM, Liedtke W, Steinhoff MS, Timmermans JP, Bunnett NW, Sharkey KA and Storr MA (2015) Transient receptor potential vanilloid 4 inhibits mouse colonic motility by activating NO-dependent enteric neurotransmission. *J Mol Med (Berl)* **93**(12): 1297-1309.
- Grynkiewicz G, Poenie M and Tsien RY (1985) A new generation of Ca²⁺ indicators with greatly improved fluorescence properties. *J Biol Chem* **260**(6): 3440-3450.
- Haynes LP, Tepikin AV and Burgoyne RD (2004) Calcium-binding protein 1 is an inhibitor of agonist-evoked, inositol 1,4,5-trisphosphate-mediated calcium signaling. *J Biol Chem* **279**(1): 547-555.
- Haynes LP, Thomas GM and Burgoyne RD (2005) Interaction of neuronal calcium sensor-1 and ADP-ribosylation factor 1 allows bidirectional control of phosphatidylinositol 4-kinase beta and trans-Golgi network-plasma membrane traffic. *J Biol Chem* **280**(7): 6047-6054.
- Kawakami K, Chiba T, Katagiri N, Saduka M, Abe K, Utsunomiya I, Hama T and Taguchi K (2012) Paclitaxel increases high voltage-dependent calcium channel current in dorsal root ganglion neurons of the rat. *J Pharmacol Sci* **120**(3): 187-195.
- Levine JD and Alessandri-Haber N (2007) TRP channels: targets for the relief of pain. *Biochim Biophys Acta* **1772**(8): 989-1003.

- Li L, Yin J, Jie PH, Lu ZH, Zhou LB, Chen L and Chen L (2013) Transient receptor potential vanilloid 4 mediates hypotonicity-induced enhancement of synaptic transmission in hippocampal slices. *CNS Neurosci Ther* **19**(11): 854-862.
- Lian LY, Pandalaneni SR, Patel P, McCue HV, Haynes LP and Burgoyne RD (2011) Characterisation of the interaction of the C-terminus of the dopamine D2 receptor with neuronal calcium sensor-1. *PLoS One* **6**(11): e27779.
- Lian LY, Pandalaneni SR, Todd PA, Martin VM, Burgoyne RD and Haynes LP (2014) Demonstration of binding of neuronal calcium sensor-1 to the cav2.1 p/q-type calcium channel. *Biochemistry* **53**(38): 6052-6062.
- Liedtke W, Choe Y, Marti-Renom MA, Bell AM, Denis CS, Sali A, Hudspeth AJ, Friedman JM and Heller S (2000) Vanilloid receptor-related osmotically activated channel (VR-OAC), a candidate vertebrate osmoreceptor. *Cell* **103**(3): 525-535.
- Mamenko M, Zaika OL, Boukelmoune N, Berrout J, O'Neil RG and Pochynyuk O (2013) Discrete control of TRPV4 channel function in the distal nephron by protein kinases A and C. *J Biol Chem* **288**(28): 20306-20314.
- Materazzi S, Fusi C, Benemei S, Pedretti P, Patacchini R, Nilius B, Prenen J, Creminon C, Geppetti P and Nassini R (2012) TRPA1 and TRPV4 mediate paclitaxel-induced peripheral neuropathy in mice via a glutathione-sensitive mechanism. *Pflugers Arch* **463**(4): 561-569.
- Matsumura Y, Yokoyama Y, Hirakawa H, Shigeto T, Futagami M and Mizunuma H (2014) The prophylactic effects of a traditional Japanese medicine, goshajinkigan, on paclitaxel-induced peripheral neuropathy and its mechanism of action. *Mol Pain* **10**: 61.

- Mielke S, Sparreboom A and Mross K (2006) Peripheral neuropathy: a persisting challenge in paclitaxel-based regimes. *Eur J Cancer* **42**(1): 24-30.
- Mo M, Erdelyi I, Szigeti-Buck K, Benbow JH and Ehrlich BE (2012) Prevention of paclitaxel-induced peripheral neuropathy by lithium pretreatment. *FASEB J* **26**(11): 4696-4709.
- Montell C, Birnbaumer L and Flockerzi V (2002) The TRP channels, a remarkably functional family. *Cell* **108**(5): 595-598.
- Ng E, Varaschin RK, Su P, Browne CJ, Hermainski J, Foll BL, Pongs O, Liu F, Trudeau LE, Roder JC and Wong AH (2015) Neuronal calcium sensor-1 deletion in the mouse decreases motivation and dopamine release in the nucleus accumbens. *Behav Brain Res.*
- Nguyen LD, Petri ET, Huynh LK and Ehrlich BE (2019) Characterization of NCS1-InsP3R1 interaction and its functional significance. *J Biol Chem* **294**(49): 18923-18933.
- Nilius B, Vriens J, Prenen J, Droogmans G and Voets T (2004) TRPV4 calcium entry channel: a paradigm for gating diversity. *Am J Physiol Cell Physiol* **286**(2): C195-205.
- Nilius B, Watanabe H and Vriens J (2003) The TRPV4 channel: structure-function relationship and promiscuous gating behaviour. *Pflugers Arch* **446**(3): 298-303.
- Pachman DR, Barton DL, Watson JC and Loprinzi CL (2011) Chemotherapy-induced peripheral neuropathy: prevention and treatment. *Clin Pharmacol Ther* **90**(3): 377-387.

- Pandalaneni S, Karuppiah V, Saleem M, Haynes LP, Burgoyne RD, Mayans O, Derrick JP and Lian LY (2015) Neuronal Calcium Sensor-1 Binds the D2 Dopamine Receptor and G-protein-coupled Receptor Kinase 1 (GRK1) Peptides Using Different Modes of Interactions. *J Biol Chem* **290**(30): 18744-18756.
- Peng H, Lewandrowski U, Muller B, Sickmann A, Walz G and Wegierski T (2010) Identification of a Protein Kinase C-dependent phosphorylation site involved in sensitization of TRPV4 channel. *Biochem Biophys Res Commun* **391**(4): 1721-1725.
- Phan MN, Leddy HA, Votta BJ, Kumar S, Levy DS, Lipshutz DB, Lee SH, Liedtke W and Guilak F (2009) Functional characterization of TRPV4 as an osmotically sensitive ion channel in porcine articular chondrocytes. *Arthritis Rheum* **60**(10): 3028-3037.
- Romero-Pozuelo J, Dason JS, Mansilla A, Banos-Mateos S, Sardina JL, Chaves-Sanjuan A, Jurado-Gomez J, Santana E, Atwood HL, Hernandez-Hernandez A, Sanchez-Barrena MJ and Ferrus A (2014) The guanine-exchange factor Ric8a binds to the Ca(2)(+) sensor NCS-1 to regulate synapse number and neurotransmitter release. *J Cell Sci* **127**(Pt 19): 4246-4259.
- Rowinsky EK, Jiroutek M, Bonomi P, Johnson D and Baker SD (1999) Paclitaxel steady-state plasma concentration as a determinant of disease outcome and toxicity in lung cancer patients treated with paclitaxel and cisplatin. *Clin Cancer Res* **5**(4): 767-774.

- Saifeddine M, El-Daly M, Mihara K, Bunnett NW, McIntyre P, Altier C, Hollenberg MD and Ramachandran R (2015) GPCR-mediated EGF receptor transactivation regulates TRPV4 action in the vasculature. *Br J Pharmacol* **172**(10): 2493-2506.
- Sanchez JC, Munoz LV and Ehrlich BE (2020) Modulating TRPV4 channels with paclitaxel and lithium. *Cell Calcium* **91**: 102266.
- Sarosy GA, Hussain MM, Seiden MV, Fuller AF, Nikrui N, Goodman A, Minasian L, Reed E, Steinberg SM and Kohn EC (2010) Ten-year follow-up of a phase 2 study of dose-intense paclitaxel with cisplatin and cyclophosphamide as initial therapy for poor-prognosis, advanced-stage epithelial ovarian cancer. *Cancer* **116**(6): 1476-1484.
- Schiff PB, Fant J and Horwitz SB (1979) Promotion of microtubule assembly in vitro by taxol. *Nature* **277**(5698): 665-667.
- Schlecker C, Boehmerle W, Jeromin A, DeGray B, Varshney A, Sharma Y, Sziget-Buck K and Ehrlich BE (2006) Neuronal calcium sensor-1 enhancement of InsP3 receptor activity is inhibited by therapeutic levels of lithium. *J Clin Invest* **116**(6): 1668-1674.
- Strotmann R, Schultz G and Plant TD (2003) Ca²⁺-dependent potentiation of the nonselective cation channel TRPV4 is mediated by a C-terminal calmodulin binding site. *J Biol Chem* **278**(29): 26541-26549.
- Takahashi N, Hamada-Nakahara S, Itoh Y, Takemura K, Shimada A, Ueda Y, Kitamata M, Matsuoka R, Hanawa-Suetsugu K, Senju Y, Mori MX, Kiyonaka S, Kohda D, Kitao A, Mori Y and Suetsugu S (2014) TRPV4 channel activity is modulated by direct interaction of the ankyrin domain to PI(4,5)P(2). *Nat Commun* **5**: 4994.

- Thorneloe KS, Sulpizio AC, Lin Z, Figueroa DJ, Clouse AK, McCafferty GP, Chendrimada TP, Lashinger ES, Gordon E, Evans L, Misajet BA, Demarini DJ, Nation JH, Casillas LN, Marquis RW, Votta BJ, Sheardown SA, Xu X, Brooks DP, Laping NJ and Westfall TD (2008) N-((1S)-1-[[4-((2S)-2-[[[(2,4-dichlorophenyl)sulfonyl]amino}-3-hydroxypropanoyl)-1 -piperazinyl]carbonyl]-3-methylbutyl)-1-benzothiophene-2-carboxamide (GSK1016790A), a novel and potent transient receptor potential vanilloid 4 channel agonist induces urinary bladder contraction and hyperactivity: Part I. *J Pharmacol Exp Ther* **326**(2): 432-442.
- Vriens J, Appendino G and Nilius B (2009) Pharmacology of vanilloid transient receptor potential cation channels. *Mol Pharmacol* **75**(6): 1262-1279.
- Wang CY, Yang F, He X, Chow A, Du J, Russell JT and Lu B (2001) Ca(2+) binding protein frequenin mediates GDNF-induced potentiation of Ca(2+) channels and transmitter release. *Neuron* **32**(1): 99-112.
- Wang MS, Davis AA, Culver DG, Wang Q, Powers JC and Glass JD (2004) Calpain inhibition protects against Taxol-induced sensory neuropathy. *Brain* **127**(Pt 3): 671-679.
- Watanabe H, Vriens J, Janssens A, Wondergem R, Droogmans G and Nilius B (2003a) Modulation of TRPV4 gating by intra- and extracellular Ca²⁺. *Cell Calcium* **33**(5-6): 489-495.
- Watanabe H, Vriens J, Prenen J, Droogmans G, Voets T and Nilius B (2003b) Anandamide and arachidonic acid use epoxyeicosatrienoic acids to activate TRPV4 channels. *Nature* **424**(6947): 434-438.

- Weiss JL and Burgoyne RD (2002) Sense and sensibility in the regulation of voltage-gated $\text{Ca}(2+)$ channels. *Trends Neurosci* **25**(10): 489-491.
- Weiss JL, Hui H and Burgoyne RD (2010) Neuronal calcium sensor-1 regulation of calcium channels, secretion, and neuronal outgrowth. *Cell Mol Neurobiol* **30**(8): 1283-1292.
- Winters-Stone KM, Hilton C, Luoh S-W, Jacobs P, Faithfull S and Horak FB (2016) Comparison of physical function and falls among women with persistent symptoms of chemotherapy-induced peripheral neuropathy. *J Clin Oncol* **34**(Supplement 3S): 1.
- Yan J, Leal K, Magupalli VG, Nanou E, Martinez GQ, Scheuer T and Catterall WA (2014) Modulation of $\text{CaV}2.1$ channels by neuronal calcium sensor-1 induces short-term synaptic facilitation. *Mol Cell Neurosci* **63**: 124-131.
- Zheng X, Zinkevich NS, Gebremedhin D, Gauthier KM, Nishijima Y, Fang J, Wilcox DA, Campbell WB, Gutterman DD and Zhang DX (2013) Arachidonic acid-induced dilation in human coronary arterioles: convergence of signaling mechanisms on endothelial TRPV4-mediated Ca^{2+} entry. *J Am Heart Assoc* **2**(3): e000080.
- Zozulya S, Ladant D and Stryer L (1995) Expression and characterization of calcium-myristoyl switch proteins. *Methods Enzymol* **250**: 383-393.

FUNDING FOOTNOTE

BEE is a co-founder of Osmol Therapeutics that is targeting NCS1 for therapeutic purposes. JCS has no conflict of interest.

FIGURE LEGENDS

Figure 1. A. Representative RT-PCR showing the expression of TRPV4 mRNA in CTR, KD and OE MDA-MB231 cells. Human β -actin was amplified as a control. Note the different levels of expression in the three different MDA-MB231 cell lines. B. Comparative expression levels of TRPV4 gene in CTR, KD and OE MDA-MB231 cells, measured by RT-qPCR. * denotes significant decrease ($p=0.0001$) comparing with CTR cells and ** denotes significant increase ($p=0.0001$) comparing with CTR cells. C. Representative Western blot showing the expression of TRPV4 and NCS1 proteins in the same cell lines in two different batches of cells. Human β -actin was used as a control. Note the different protein levels in the three different MDA-MB231 cell lines. The arrow indicates the TRPV4 band used to quantify the level of expression. D. Comparative levels of TRPV4 and NCS1 expression in MDA-MB231 cells normalized to levels of β -actin expression ($n=8$). * denotes significant decrease ($p=0.0001$) comparing with CTR cells and ** denotes significant increase ($p=0.0001$) comparing with CTR cells. E. Representative Western blot showing the expression of TRPV4, β -actin and NCS1 proteins in MDA-MB231, in control conditions (two columns on the left) and following a PTX 6-hour treatment (two columns on the right), in two different batches of cells. The arrow indicates the TRPV4 band used to quantify the level of expression. Note the different TRPV4 and NCS1 protein levels after PTX treatment. F. Comparative levels of TRPV4 and NCS1 expression in CTR MDA-MB231 cells, as indicated in A. $n=8$ in all cases. * denotes significant increase ($p<0.0169$) and ** denotes significant decrease ($p<0.0012$).

Figure 2. A. Representative Western blot following co-immunoprecipitation as indicated, in CTR MDA-MB231 cells. B. Representative Western blot following co-immunoprecipitation as indicated, in CTR MDA-MB231 cells in the presence of PTX. Note that the non-identified bigger bands correspond to the antibody heavy and light chains in both A and B panels.

Figure 3. A. Typical I-V recording of the current obtained in individual CTR, KD and OE MDA-MB231 cells, elicited by a ramp protocol from -100 mV to +100 mV and activated by GSK101. Note the trace in CTR cells in the presence of HC-067047. B. I-V relationship of the GSK101-induced current in CTR, KD and OE MDA-MB231 cells. C. Comparison between the mean maximal normalized GSK101-induced current recorded at -60 mV and +60 mV in the three different cell lines as indicated in B and in CTR cells in the presence of HC-067047. D. Comparison between the mean maximal normalized GSK101-induced current recorded at -60 mV and +60 mV in the presence of 50 nM HC-067047 in the three different cell lines. Note that the current was also almost completely inhibited. n= 12 in all cases. * denotes significant current increase (inward p=0.0001; outward p=0.0239) and ** denotes significant current decrease (inward p=0.0053; outward p=0.0032).

Figure 4. A. I-V relationship of the TRPV4 currents in CTR MDA-MB231 cells in basal conditions and in the presence of PTX (1-minute exposure), as indicated. n=10 in all cases. B. Recordings at -60 mV and +60 mV in CTR MDA-MB231 cells in the same

conditions described in A, as indicated. In all the traces shown the baseline was adjusted to zero to subtract the minimal resting current. A recording made in the presence of HC067047 is showed as a negative control. The smallest arrow indicates the point at which PTX was added, the middle size arrow indicates the point in which GSK101 was added and the largest arrow indicates the point of wash-out of PTX and GSK101. C. Comparison of the mean maximal current recorded in MDA-MB231 (CTR, KD and OE) cells at -60 mV and $+60$ mV, following 1-minute exposure PTX, as indicated. Open bars are control, black bars are +PTX. D. Comparison of the mean maximal current recorded in MDA-MB231 (CTR, KD and OE) cells at -60 mV and $+60$ mV, following 6-hour exposure PTX, as indicated. Open bars are control, black bars are +PTX. n is indicated in each case. * denotes significant current increase at 1-minute exposure (CTR inward $p=0.0001$; CTR outward $p=0.0003$; OE inward $p=0.0001$; OE outward $p=0.0004$) and at 6-hours exposure (CTR inward $p=0.0001$; CTR outward $p=0.0001$; OE inward $p=0.0039$; OE outward $p=0.0005$) in comparison to control. Note that there was no effect on KD cells.

Figure 5. A. Recordings of single channel activity (opening is downward) and corresponding amplitude histogram of single-channel currents in basal conditions in inside-out patches from CTR MDA-MB231 cells. B. Recordings of single channel activity (opening is downward) and corresponding amplitude histogram of single-channel currents through TRPV4, activated by GSK101. C. Recordings of single channel activity (opening is downward) and corresponding amplitude histogram of single-channel currents through TRPV4, activated by GSK101, in the presence of $10\text{ }\mu\text{M}$ NCS1. D.

Comparison of the mean open probability (P_o) in 10 different patches in the three conditions described in A, B and C. * denotes significant increase in comparison to control ($p=0.0001$) and ** denotes significant increase in comparison to control and GSK101 alone ($p=0.001$). E. Single-channel I-V relationship from 10 different patches per voltage for the currents elicited by GSK101 in the absence and the presence of NCS1 (black line is CTR, gray line is +NCS1). From linear regressions, an inward conductance and outward conductance were calculated for each condition, as indicated. F. Comparison of the mean conductance in 10 different patches in the absence and the presence of NCS1. * denotes significant increase (inward $p=0.0053$; outward $p=0.0014$).

Figure 6. A. Recordings of single channel activity (opening is downward) and corresponding amplitude histogram of single-channel currents in basal conditions in inside-out patches from SH-SY5Y cells. B. Recordings of single channel activity (opening is downward) and corresponding amplitude histogram of single-channel currents through TRPV4, activated by GSK101. C. Recordings of single channel activity (opening is downward) and corresponding amplitude histogram of single-channel currents through TRPV4, activated by GSK101, in the presence of 10 μ M NCS1. D. Comparison of the mean open probability (P_o) in 10 different patches in the three conditions described in A, B and C. * denotes significant increase in comparison to control ($p=0.0001$) and ** denotes significant increase in comparison to control and GSK101 alone ($p=0.001$). E. Single-channel I-V relationship from 8 different patches per voltage for the currents elicited by GSK101 in the absence and the presence of NCS1 (black line is CTR, gray line is +NCS1). From linear regressions, an inward conductance

and outward conductance were calculated for each condition, as indicated. F. Comparison of the mean conductance in 8 different patches in the absence and the presence of NCS1. * denotes significant increase (inward $p=0.0001$; outward $p=0.0001$).

Figure 7. Recordings of single channel activity (opening is downward) and corresponding amplitude histogram of single-channel currents through TRPV4, activated by GSK101, in the presence of PTX alone (A) and in the presence of PTX and NCS1 (B) in inside-out patches from CTR MDA-MB231. C. Comparison of the mean open probability (P_o) in 12 different patches in the conditions described in A and B, as indicated. * denotes significant increase ($p=0.0387$). D. Comparison of the mean inward and outward conductances in 10 different patches in the conditions described in A and B, as indicated; conductances were calculated from linear regressions of the corresponding I-V relationships. * denotes significant increase (inward $p=0.0111$; outward $p=0.0065$).

Figure 8. Recordings of single channel activity (opening is downward) and corresponding amplitude histogram of single-channel currents through TRPV4, activated by GSK101, in the presence of PTX alone (A) and in the presence of PTX and NCS1 (B) in inside-out patches from SH-SY5Y. C. Comparison of the mean open probability (P_o) in 10 different patches in the conditions described in A and B, as indicated. * denotes significant increase ($p=0.0044$). D. Comparison of the mean inward and outward conductances in 10 different patches in the conditions described in A and B, as indicated; conductances were calculated from linear regressions of the

corresponding I-V relationships. * denotes significant increase (inward $p=0.0021$; outward $p=0.0001$).

Figure 9. A. Representative recordings of intracellular Ca^{2+} concentration in Fura-2-loaded MDA-MB231 (CTR, KD and OE) cells in steady-state conditions and following GSK101 treatment. Fluorescence was recorded for 150 s. The arrow indicates the moment in which GSK101 was added to the external solution. B. Representative recordings of intracellular Ca^{2+} concentration in Fura-2-loaded MDA-MB231 CTR cells in steady-state conditions and following GSK101 treatment in the presence of HC-067047, in Tg pre-treated cells (Tg) and in Ca^{2+} -free external solution. Fluorescence was recorded for 150 s. The arrow indicates the moment in which GSK101 was added to the external solution. Note that there was no response to GSK101 in the presence of HC-067047 or in Ca^{2+} -free external solution. C. Comparison between mean maximal GSK101-induced intracellular Ca^{2+} increase percentage in Fura-2-loaded MDA-MB231 cells (CTR, KD, OE), in the presence of HC-067047, in Tg pre-treated cells (Tg) and in Ca^{2+} -free external solution. n is indicated in each case. * denotes a significant Ca^{2+} decrease ($p=0.0001$ in all cases). D. Comparison between mean maximal GSK101-induced intracellular Ca^{2+} increase percentage in Fura-2-loaded MDA-MB231 cells (CTR, KD, OE) in 1-min and 6-hour PTX exposure, as marked. n is indicated in each case. * denotes significant Ca^{2+} increase in comparison to control (CTR $p=0.0038$; OE $p=0.0276$) and ** denotes significant Ca^{2+} increase in comparison to control and 1-min exposure (CTR $p=0.0038$; OE $p=0.0276$). Note that there was no effect on KD cells.

Figure 1

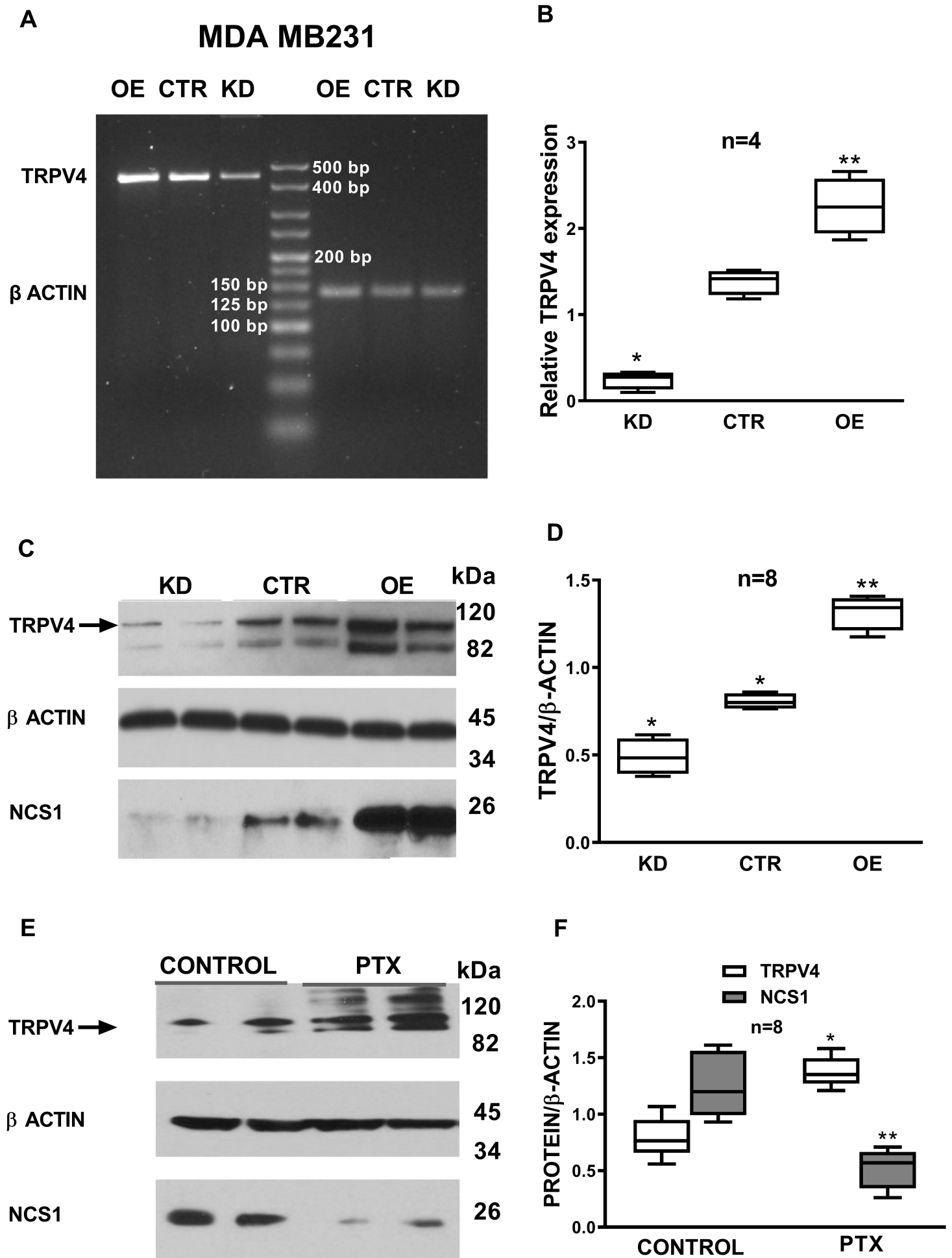


Figure 2

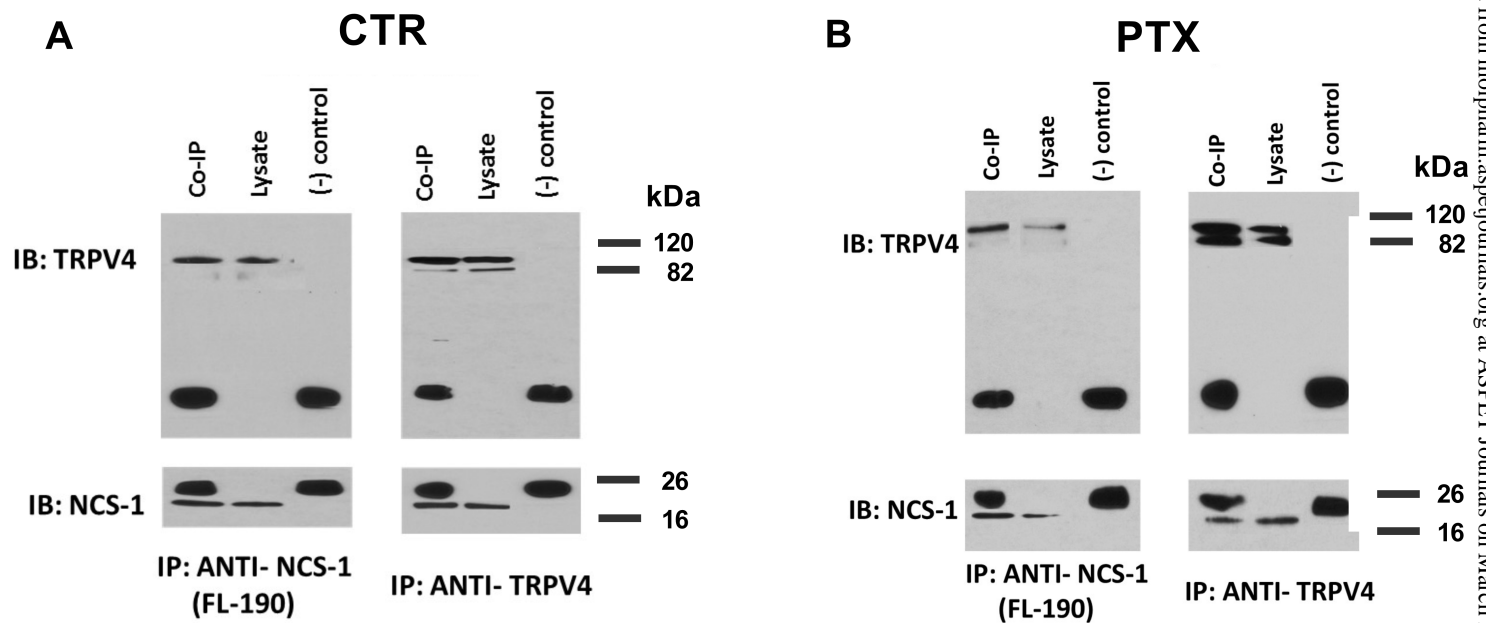


Figure 3

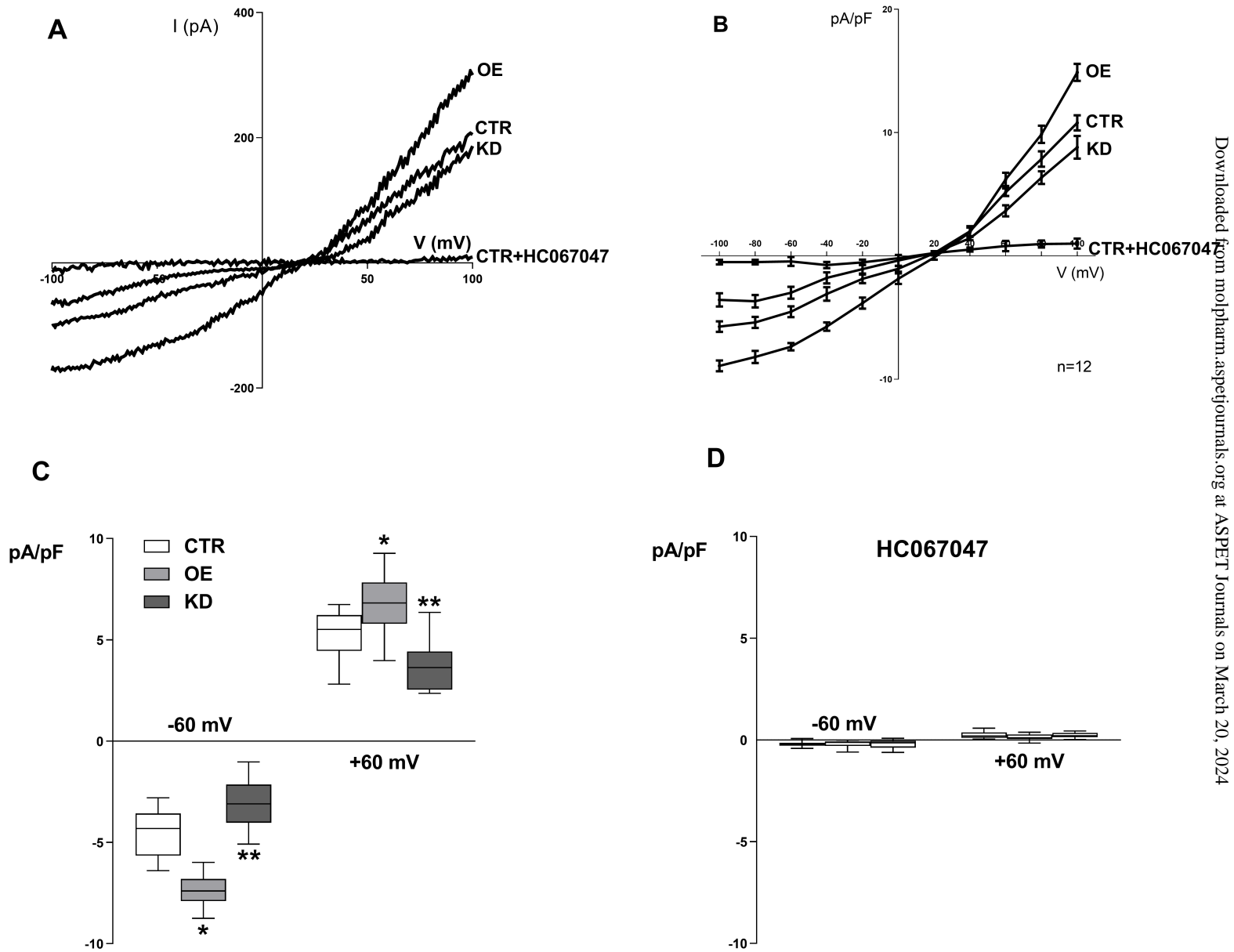


Figure 4

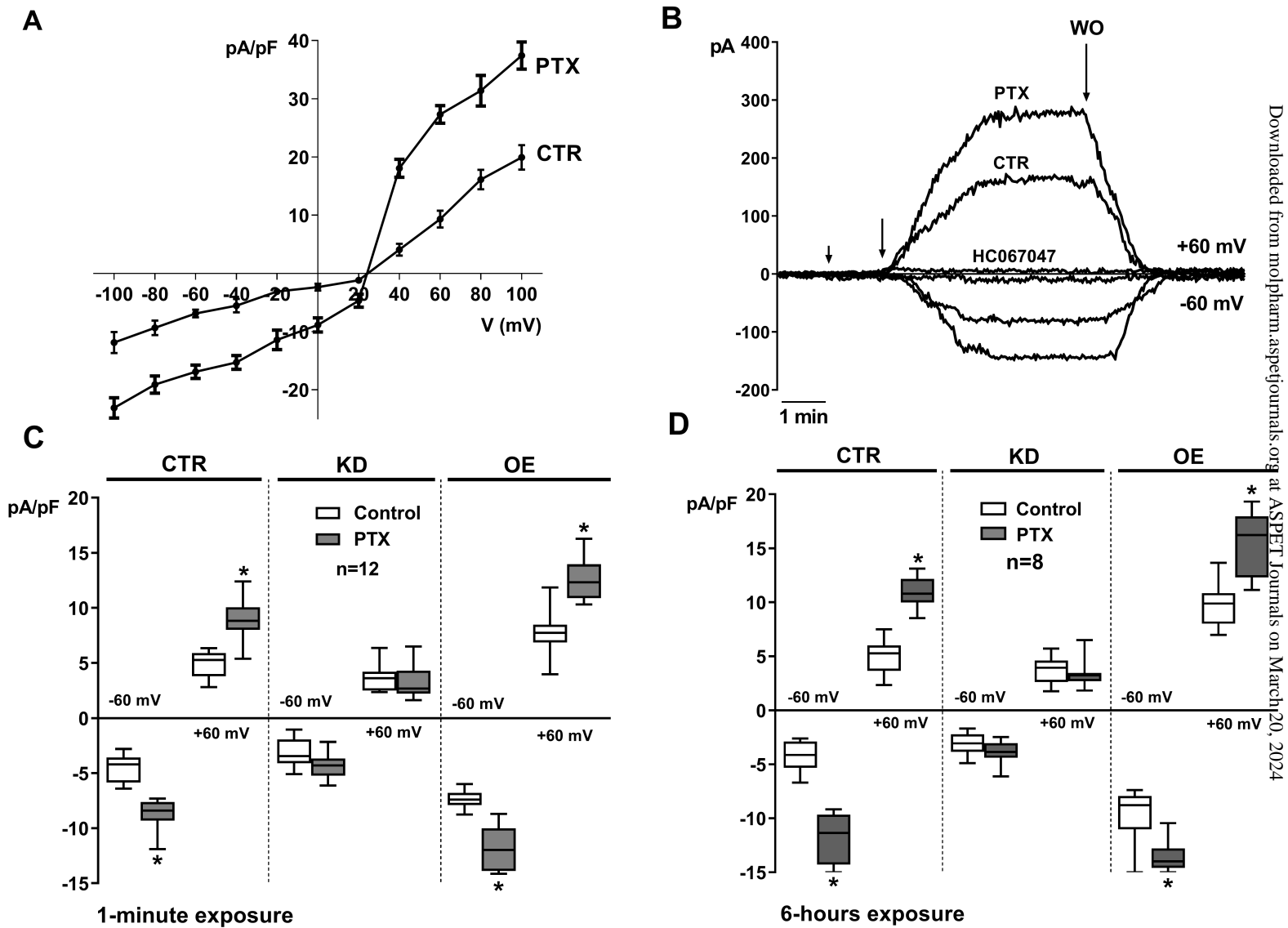
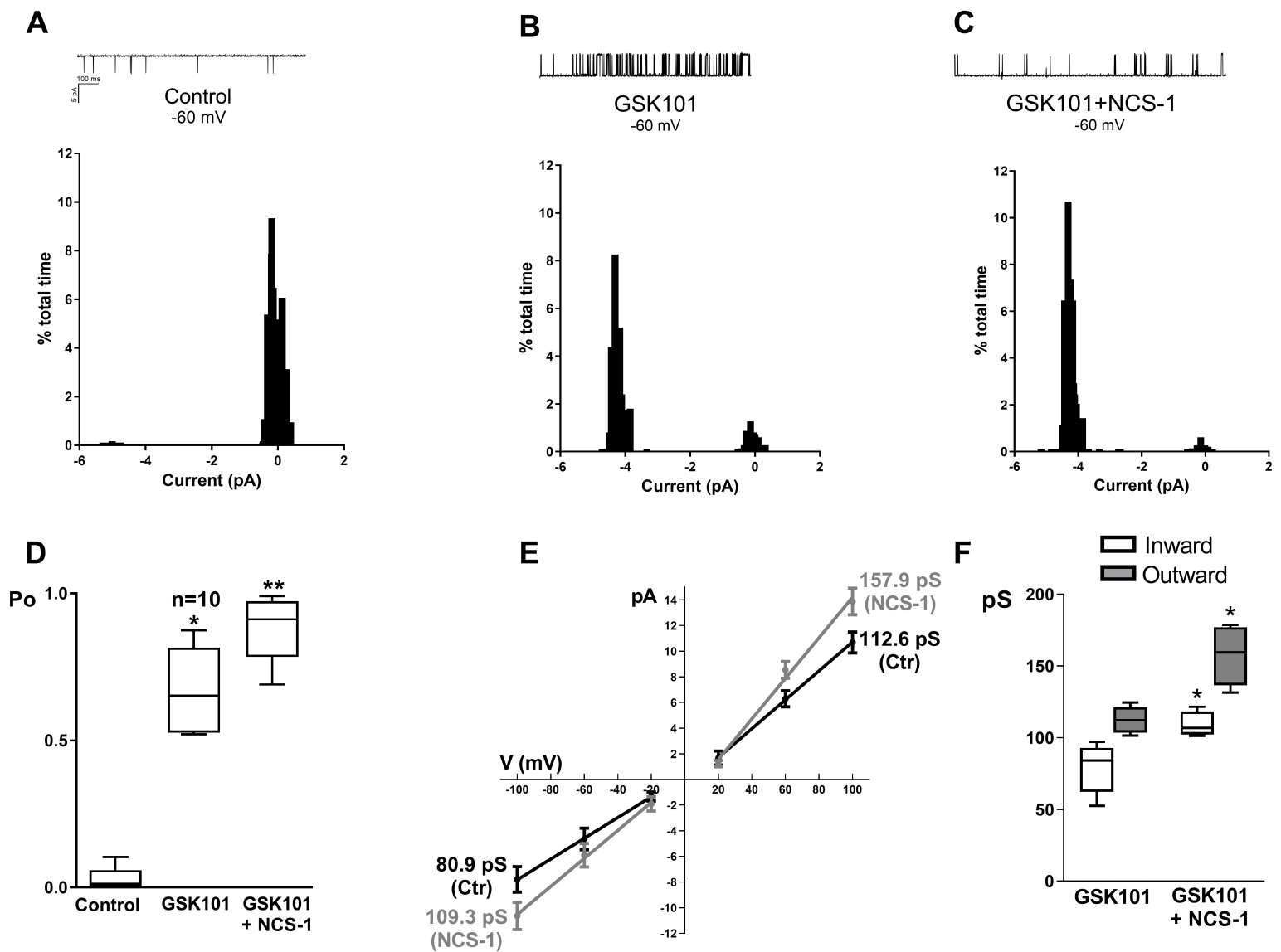
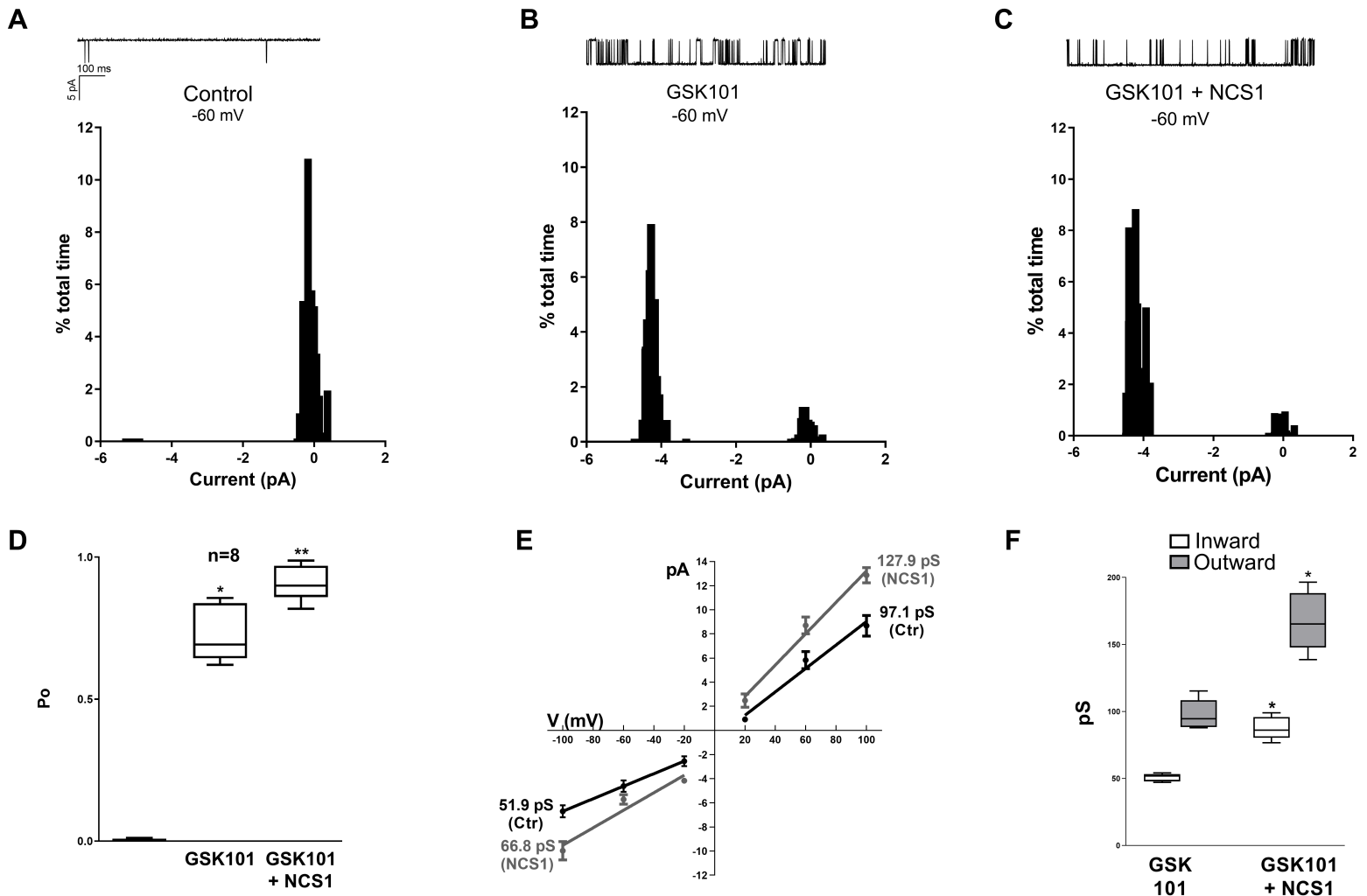


Figure 5



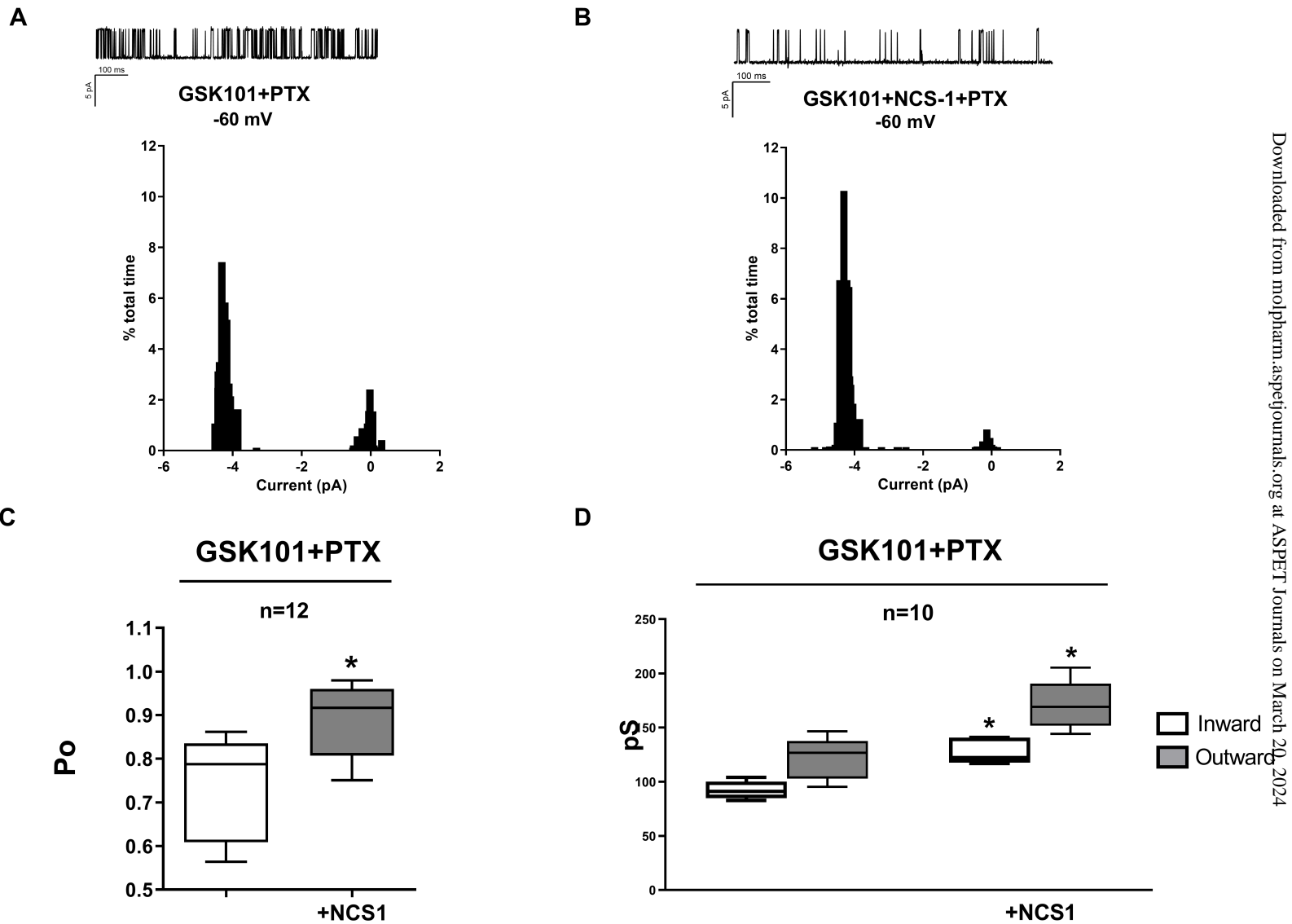
MDA-MB231

Figure 6



SH-SY5Y

Figure 7



MDA-MB231

Figure 8

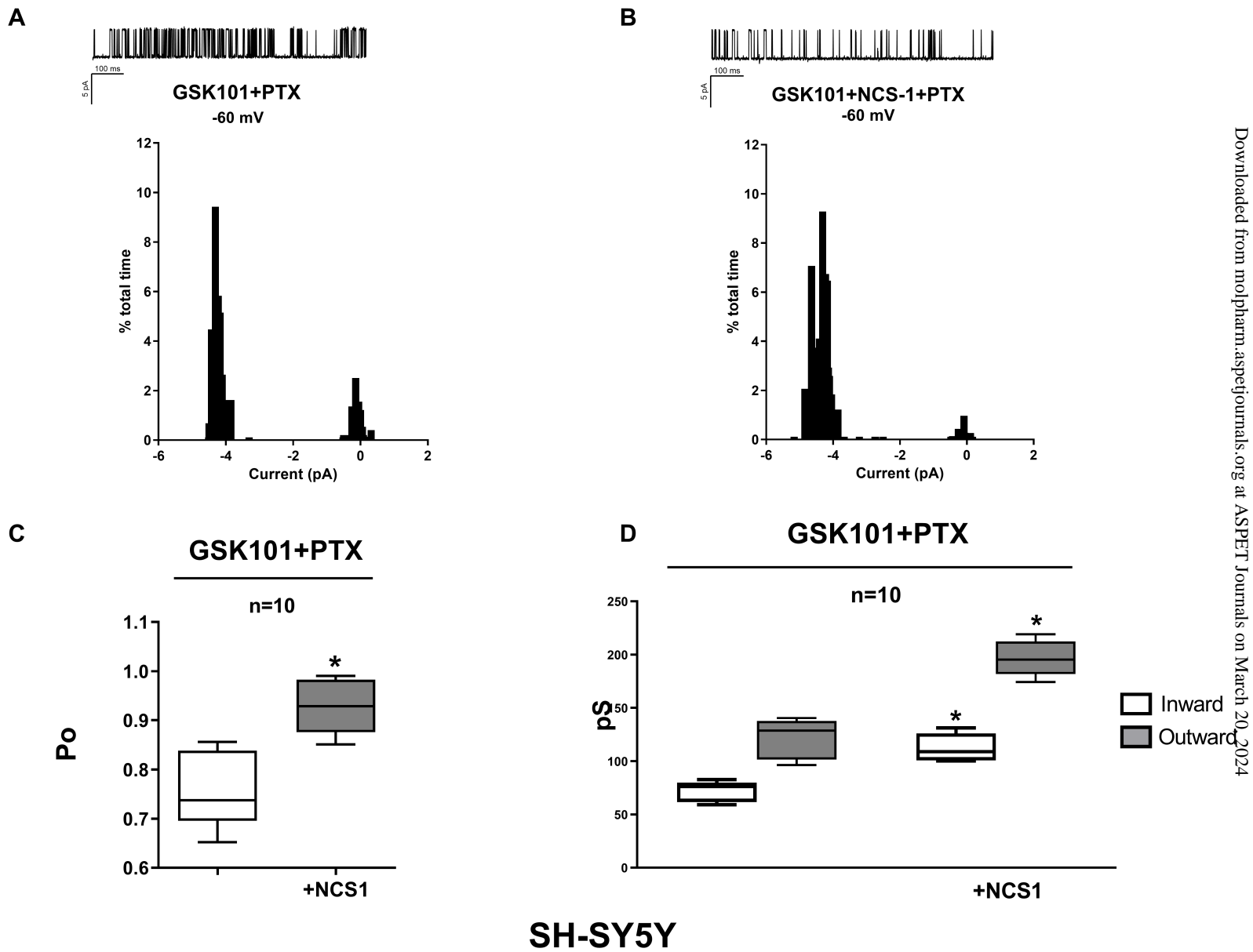


Figure 9

